2D Graphene-Like Carbon Coated Solid Electrolyte for Reducing Inhomogeneous Reactions of All-Solid-State Batteries

Hyeon-Ji Shin, Jun-Tae Kim, Daseul Han, Hyung-Seok Kim, Kyung Yoon Chung, Junyoung Mun, Jongsoon Kim, Kyung-Wan Nam, and Hun-Gi Jung*

Recent studies have identified an imbalance between the electronic and ionic conductivities as the drivers of inhomogeneous reactions in composite cathodes, which cause the rapid degradation of all-solid-state battery (ASSB). To mitigate localized overcharge and utilize isolated active materials, the study proposes the coating of an argyrodite-type Li_6PS_5Cl solid electrolyte (SE) with graphene-like carbon (GLC@LPSCl), a 2D conductive material, to offer a continuous three-dimensionally connected electron pathway within the composite cathode to facilitate ion mobility and promote homogeneous reactions. Despite reducing the content of the conducting agent, it is observed that the GLC@LPSCl cell exhibits high initial Coulombic efficiency and discharge capacity, reducing the inhomogeneous reactivity after 200 cycles compared with when ordinary conductive agents are deployed. Additionally, the presence of GLC@LPSCl surface suppresses the interfacial reaction between SE–cathode material, thus imparting the cell with excellent capacity retention (≈90%) after 200 cycles. Furthermore, the cell performance improves even after a fourfold increase in the cathode loading amount, demonstrating the criticality of a well-developed continuous electron pathway to cell performance and highlighting the key role of ensuring a balance between the electron and ion conductivities in the development of high-energy-density and high-power ASSBs.

1. Introduction

As part of efforts to address climate change, the development of Li secondary batteries with high-energy densities and high power that can facilitate the transition from internal combustion engines to electrified vehicles has become the focus of most studies in the last decades. Recently, all-solid-state batteries (ASSBs) were rapidly developed to circumvent the existing safety issues of batteries, such as explosions and fires.[1,2] Additionally, among various solid electrolytes (SEs) for ASSBs, sulfide-based SEs exhibiting high Li-ion conductivity are advantageous, as they can increase the energy density; thus, they have efficiently improved the performances of ASSBs over the past few years.[3–5] By applying Ni-rich $LiNi_xMn_yC_{1-x-y}O_2$ (x ≥ 0.6) cathode active materials (CAM) to sulfide-based ASSBs and improving the cell manufacturing technology for μ-Si, Li metal, or anode-free systems, researchers

H.-J. Shin, J.-T. Kim, H.-S. Kim, K. Y. Chung, H.-G. Jung
Energy Storage Research Center
Sustainable Energy Research Division
Korea Institute of Science and Technology
Seoul 02792, South Korea
E-mail: hungi@kist.re.kr
J.-T. Kim
Department of Energy Engineering
Hanyang University
Seoul 04763, South Korea
D. Han, K.-W. Nam
Department of Energy and Materials Engineering
Dongguk University
Seoul 04620, South Korea

The ORCID identification number(s) for the author(s) of this article can be found under https://doi.org/10.1002/aenm.202403247

H.-S. Kim, K. Y. Chung, H.-G. Jung
Division of Energy and Environment Technology
KIST School, University of Science and Technology
Seoul 02792, South Korea
J. Mun
School of Advanced Materials Science and Engineering
Sungkyunkwan University
Suwon 16419, South Korea
J. Kim, H.-G. Jung
Department of Energy Science
Sungkyunkwan University
Suwon 16419, South Korea
H.-G. Jung
KIST-SKKU Carbon-Neutral Research Center
Sungkyunkwan University
Suwon 16419, South Korea

**ADVANCED
SCIENCE NEWS**

www.advancedsciencenews.com

**ADVANCED
ENERGY
MATERIALS**

www.advenergymat.de

have developed high-capacity batteries of ≥ 5 mAh cm^{-2}.[6,7] Moreover, the commercialization of ASSBs has been significantly boosted by the advancements in the manufacturing technologies for large-area electrodes as well as the introduction of pouch-type cells.

To suppress interfacial degradation, which increases cell resistance or degrades cell performance, the performances of ASSBs have been improved by optimizing the materials deployed in each component. First, regarding the SE–Li metal anode interface, a high-performance all-solid-state lithium metal battery was developed by stabilizing the SE–Li metal interface. In addition to a pore-filling SE, a composite SE, compounded from polyvinylidene fluoride with materials such as sodium doped LiFePO$_4$ or Li$_4$Ti$_5$O$_{12}$, were effectively suppressed Li dendrite growth and minimized interfacial resistance.[8–10] Representative approaches include coating the surface of CAM with an ionic conductive layer or a bandgap-alleviating layer or introducing a doped or substituted SE with superior ionic conductivity.[11–18] Recent studies have analyzed and elucidated the material and macroscopic issues of ASSBs, such as inhomogeneous reactions within composite electrodes.[19–24] These inhomogeneous reactions due to loosely contacting and isolated active materials have been confirmed by transmission X-ray microscopy with X-ray absorption near-edge structures (TXM–XANES).[20] Additionally, 3D *operando* computed tomography–XANES and in situ transmission electron microscopy (TEM) have revealed that slow ion transport via active material particles, particularly slow diffusion through CAM nanocrystal boundaries, significantly restricts Li conductivity, resulting in inhomogeneous reactions.[21,22] Thus, the inhomogeneous reactions within the composite electrode decrease the capacity and rate capabilities of ASSBs, facilitating local overcharge–discharge and ultimately degrading cell performance.

In the absence of a solution to the inhomogeneous reactions within electrodes, the capacity and lifespan degradation issues become more severe when thickening the electrode for high-energy-density batteries.[21,25,26] Inhomogeneous reactions have been studied in liquid-electrolyte-based Li-ion batteries. They are caused by an imbalance between the electronic and ionic conductivities of batteries owing to inhomogeneous and insufficient charge transfers. Thus, the phenomenon can cause more severe performance degradation, especially in thick electrode.[27,28] Therefore, to improve the electronic–ionic conductivity balance of batteries, different dimensions of carbon, such as carbon nanotubes (one-dimensional, 1D) and graphene (Gr, 2D), have been mixed to generate well-developed electron-percolating pathways.[29,30] Additionally, the electrochemical properties of these batteries have been improved by applying conformal Gr coatings to CAM via the Pickering emulsion method, thus increasing the CAM content to more than 98% and improving the volumetric and specific-capacity limits.[31] Regarding ASSBs, their inhomogeneous reactivity becomes very noticeable when their electrodes are thickened to produce high-energy-density and high-power-density batteries; as with other batteries, this significant reactivity rapidly degrades the cell performance. Therefore, facilitating adequate Li-ion diffusion within composite electrodes and providing sufficient electron-transfer pathways can improve the cell performance and inhibit inhomogeneous reactions electrodes.

To facilitate sufficient ion transport even at high current density, an appropriate amount of a conductive agent must be applied and homogeneously distributed. In most electrode manufacturing processes, carbon materials are added as conductive agents to generate an electron-mobility pathway. As carbon exhibits very low density and high volumetric properties, only small amounts are required to facilitate sufficient charge transfer in the composite cathode. Sulfide-based ASSBs typically deploy 0D-type carbon black, such as Super P, Super C65, and acetylene black, and 1D-type carbon nanofibers or vapor-grown carbon fibers (VGCFs).[32–35] Unfortunately, 0D carbons cannot readily form continuous pathways with solid–solid point contact and 1D carbons tangle with each other, complicating their physical uniform dispersion. Additionally, studies have revealed that the presence of ordinary carbon conductive agents in composite cathodes majorly causes an increase in interfacial resistance by promoting undesirable side reactions, such as SE decomposition.[34,36] Therefore, their addition is not an ideal strategy for simply increasing the carbon content toward improving electronic conductivity. Park et al. recently reported that carbon accelerates SE decomposition because of the presence of an O-containing functional group on amorphous carbon surfaces.[33] They demonstrated that removing the functional groups as well as changing the carbon black surface into a few-layered graphitic carbon by a simple heat treatment at 1200 °C improved the initial capacity and cycling characteristics by suppressing the CAM–SE side reaction.

Although the suppression of interfacial degradation is key to improving the energy density and electrochemical properties of sulfide-based ASSBs, mitigating their inhomogeneous reactivity may be more crucial. Thus, this study focuses on the improvement of ASSB performance by simultaneously enhancing the electron-transfer characteristics of the battery and suppressing interfacial side reactions within the composite cathode using graphitic carbon. We attempted to resolve the inhomogeneous reactivity of the battery, which might be severe in thick-film electrodes as an approach for improving the electron-transfer pathway within the composite cathode. Concurrently, we applied a graphene-like carbon (GLC), as a conductive agent to suppress interfacial side reactions, ultimately improving the capacity, rate capability, and cycling characteristics of the battery. Generally, SE is placed around the CAM regarding material distribution within the composite cathode. Therefore, coating the SE with a 2D conductive material (e.g., GLC) is a rational approach to facilitating the homogeneous and smooth transfer of electrons within the composite cathode. Here, we optimized the coating process of GLC nanopowder (GNP) on an argyrodite-type Li$_6$PS$_5$Cl (LP-SCl) SE in a simple and effective solvent-based environment, thereby enhancing the initial capacity and rate capability via the dispersed conductive agent, which generated a continuous electron pathway. Additionally, the inhomogeneous reaction was inhibited after 200 cycles via the mitigation of the local overcharge–discharge; the interfacial resistance was reduced by suppressing direct solid (SE)–solid (CAM) contact, thereby preventing SE oxidation. Overall, this study reveals that ASSB operated well with
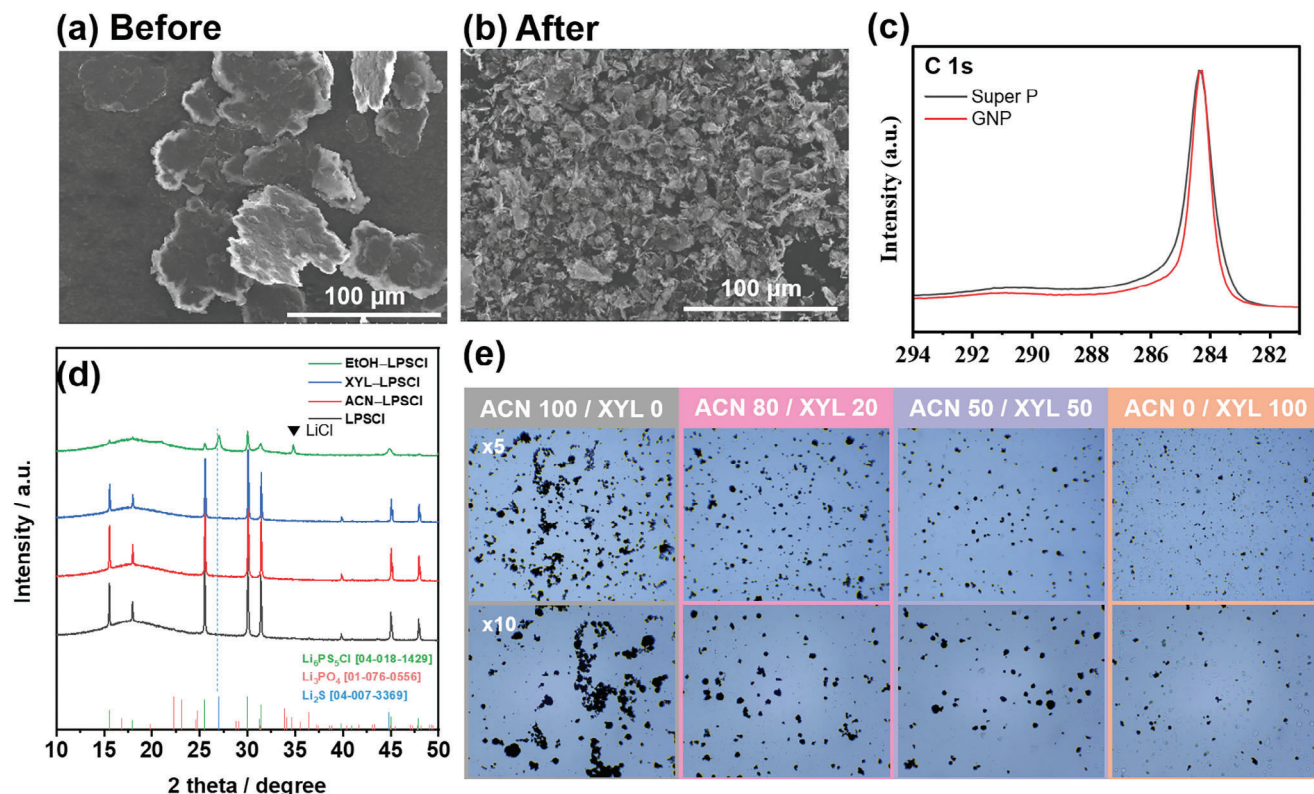
**ADVANCED
SCIENCE NEWS**

www.advancedsciencenews.com

**ADVANCED
ENERGY
MATERIALS**

www.advenergymat.de

Figure 1. SEM images of the commercial GNP a) before and b) after sonication. c) Normalized XPS spectra of the C 1s signals of ordinary conductive agents and GNP. d) XRD results of the LPSCl phase based on solvent exposure. e) OM-analysis-based comparison of the GNP dispersion based on the ACN:XYL ratio.

high CAM loading for high-energy-density functions even after modifying only the charge-transfer path within the composite electrode.

2. Results and Discussion

2.1. Optimization of the Coating Process of Graphene Nanopowders on the Argyrodite-Type Li_6PS_5Cl Solid Electrolyte

Gr is a 2D carbon type exhibiting excellent electronic conductivity, lightweight, and high strength; it can be used as a conductive agent for electrochemical energy storage devices.[37] However, the direct application of commercially available Gr to the coating is challenging because they exist as thick layers induced by self-aggregation.[31] The purchased GNP exhibited an average flake thickness and average lateral size of 5–30 nm and 5–25 μm, respectively. Additionally, X-ray diffraction (XRD) and Raman analysis results are shown in Figure S1 (Supporting Information) to provide specific information about the purchased GNP. Based on this characterization, it was found to be carbon with some defects. Therefore, we have decided to refer to the purchased Gr (GNP) as GLC. Although its thickness was good for application as a multilayer, its lateral size is too large for application as a coating layer on LPSCl. As shown in **Figure 1a**, scanning electron microscopy (SEM) was performed to confirm the morphology and size of the utilized GNP. The particle size ranged from the average size to over 40 μm, and each plate was densely stuck to the GLC sheets

with thicknesses ranging from hundreds of nm to 2–3 μm. As this dense particle could not be readily separated into a thin GLC layer by simple stirring in the solvent, we crushed it into smaller particles by horn sonication, thereby decreasing the average particle size (Figure 1b).

In the X-ray photoelectron spectroscopy (XPS) C 1s spectrum, we normalized the C1s spectra for both Super P and GNP to relatively compare their graphitic properties (Figure 1c). Upon normalization and full width at half maximum analysis, GNP displayed a narrower graphitic carbon peak, indicating higher crystallinity compared to Super P. Given the minimal presence of functional groups, SE oxidation is more likely due to direct contact between CAM and SE rather than any interaction with carbon's functional groups. The O-containing functional group was barely detected; thus, we predicted that it would not seriously affect sulfide SE oxidation caused by its functional group like acetylene black carbon in previous studies.[33] Therefore, SE oxidation in sulfide ASSB may be more likely to be due to direct contact between CAM and SE than to carbon's functional group.

Ball milling is often used when GLP composites or GLP coating,[38,39] therefore, we conducted GLC coating on LPSCl (GLC@LPSCl) via rotating ball milling as a preliminary experiment. In our preliminary experiment of GLC@LPSCl, we confirmed that even a small amount of GNP of less than 1 wt.% was sufficient for coating (See Figure S2, Supporting Information). However, after ball milling, the ionic conductivity of LPSCl decreased by 78% from 4.31 to 0.94 mS cm^{-1}, and the peak intensity

ADVANCED
SCIENCE NEWS

www.advancedsciencenews.com

ADVANCED
ENERGY
MATERIALS

www.advenergymat.de

in XRD decreased significantly (Figure S3a,b, Supporting Information). This is because LPSCl is fined by milling energy and the worn surface acts as a significant resistance to Li ionic conduction (Figure S3c, Supporting Information). Therefore, to avoid this, we decided to use a solvent-based coating, and therefore, it is necessary to select a suitable solvent for both the SE and GNP. Ethanol (EtOH), Acetonitrile (ACN), and Xylene (XYL), which are widely used solvents for liquid-based synthesis of LPSCl or slurry casting, were selected as solvent candidates. To determine the impact on solvent treatment, LPSCl (0.5 g) was added to the solvent (10 mL) and stirred at 25 °C for 1 h (See Figure S4, Supporting Information), followed by vacuum drying at 180 °C using the Büchi oven. The result of the XRD analysis in Figure 1d shows the phase stability of the LPSCl according to the solvent exposure. LPSCl exposed to ACN and XYL displayed the same peak position as pristine LPSCl, while LPSCl exposed to EtOH almost disappeared from the main peak, although new peaks of Li_2S and LiCl corresponding to the precursors appeared. Therefore, ACN, XYL, or a mixture of both seemed suitable as the solvent. To determine the compatibility of GNP in ACN and XYL, four solutions were prepared; ACN 100%, ACN 80%–XYL 20%, ACN 50%–XYL 50%, and XYL 100% (v/v ratio). After adding a small amount of GNP to each solution and stirring for 1 h, the degree of dispersion of GNP was measured with an optical microscopy (OM, Figure 1e). As GNP is composed of sp^2-hybridized carbon, π–π interaction with the benzene ring of XYL is possible, so XYL tends to permeate into the GLC layer more easily, resulting in smaller GNPs with a high ratio of XYL solution. However, as a result of measuring the ionic conductivity of LPSCl after solvent exposure (Figure S5, Supporting Information), when exposed to ACN, it had 4.0 mS cm^{-1} similar to that of pristine (4.31 mS cm^{-1}), while LPSCl exposed to XYL showed a significant decrease to 2.47 mS cm^{-1}. Although XYL has a good interaction with GNP, it has a large decrease in the ionic conductivity of LPSCl. Regarding the ionic conductivity of the mixture, that of the ACN 80%–XYL 20% blend was slightly higher than that of the ACN 50%–XYL 50% blend. We thought that ACN reduces the contact rate between XYL and LPSCl, thereby suppressing the decrease in ionic conductivity. Furthermore, it is anticipated that the dispersion of GNP in XYL, followed by the preparation of the XYL–ACN mixed solution and the addition of LPSCl to that solution, would facilitate GNP dispersion and LPSCl ionic conductivity retention. So, it is better to use it in combination with ACN by minimizing the content of XYL instead of alone. By combining the OM and ionic conductivity results, it was confirmed that ACN 80%–XYL 20% is the most suitable ratio for preparing GLC@LPSCl.

To obtain GLC@LPSCl, GNP, and LPSCl were mixed in an ACN 80%–XYL 20% solvent by stirring through several steps, and the representative process for each step was shown as a digital image in Figure S6 (Supporting Information). All procedures were carried out in a glovebox to avoid contamination and moisture exposure. First, add GNP to the XYL equivalent to 20 v/v % of total and sonicate it to immerse XYL between GNPs so that it is to be smaller pieces than after horn sonication.[40] At this time, the maximum GNP concentration in XYL is 4 mg mL^{-1} depending on the ratio of GNP to LPSCl, and this is acceptable because Gr including reduced graphene oxide is physically dispersed in organic solvent up to 63 mg mL^{-1}.[41] Thereafter, the remaining 80 v/v% was filled with ACN and vigorously stirred for 1 h (Figure

S6a, Supporting Information). When the mixture is sufficiently mixed and the GNPs appear to be dispersed in the solvent, LP-SCl is slowly added in portions. When a large amount of LPSCl is added at once, $[S_3]^-$ is eluted by ACN and the color of the solution turns transparent light blue as shown in Figure S3c (Supporting Information).[42] Therefore, by slowly adding LPSCl so that it immediately covers the GNPs and minimizing the exposure time to the solvent, a gray-colored dispersed solution as shown in Figure S6b (Supporting Information) can be obtained. In this regard, slowly adding LPSCl increased opportunities for physical contact between the SE particles and GNP, likely facilitating aggregation through van der Waals forces. As stirring continued, physical contact between particles increased, allowing van der Waals forces to play a more significant role than electrostatic repulsion. Under static conditions, electrostatic repulsion may dominate, but during stirring, the proximity of particles likely enabled van der Waals forces to induce aggregation. Furthermore, the dielectric properties of ACN likely contributed to shielding electrostatic interactions, allowing van der Waals forces to act more strongly. Although this mechanism was not directly verified experimentally, the observed trends and theoretical considerations suggest that van der Waals forces were the primary factor driving the formation of the GLC@LPSCl.

After sufficiently stirring the mixture, raise the temperature of the hot plate to evaporate all the solvent, and subsequently vacuum dried at 180 °C for 12 h using the Büchi Glass Oven to obtain GLC@LPSCl. The powder color obtained depended on the GNP to LPSCl weight ratio, and we prepared 1, 3, 5, 7, and 10 wt.% in the same manner as reported above (Figure S6c, Supporting Information). As a representative example, EA (CHNS) analysis was performed to confirm that the amount of GNP present in 5 wt.% GLC@LPSCl was as much as it was added (Table S1, Supporting Information). Pristine LPSCl contained 0.16 wt.% of C while 5 wt.% GLC@LPSCl contained 4.95 wt.% of C confirming that GNPs were well distributed with the SE. In line with the EA analysis, material characterization and electrochemical evaluation were conducted with 5 wt.% GLC@LPSCl, from now on, consider GLC@LPSCl as 5 wt.% GLC@LPSCl, and the reason for choosing 5 wt.% GLC@LPSCl will be discussed in detail later.

2.2. Material and Electrochemical Characterizations of the GLC@LPSCl

To confirm that the final product was obtained as expected, GLC@LPSCl was measured for material and electrochemical characterization. **Figure 2a** presents the XRD analysis results of LPSCl before and after GNP coating. No new peaks emerged, only an additional peak at 26.4° corresponding to graphitic carbon, suggesting no side reaction even when LPSCl is exposed to solvents or GNP. Through the previous XRD data, we found that there was no particular structural change in LPSCl even after solvent exposure and GNP contact during the GLC@LPSCl manufacturing process. However, since XRD shows average structural information, it is difficult to obtain information on local structure changes on the surface of the material that was directly exposed to solvent and GNP. Therefore, short-range ordering was confirmed through pair distribution function (PDF) analysis based on synchrotron X-ray scattering data. As shown
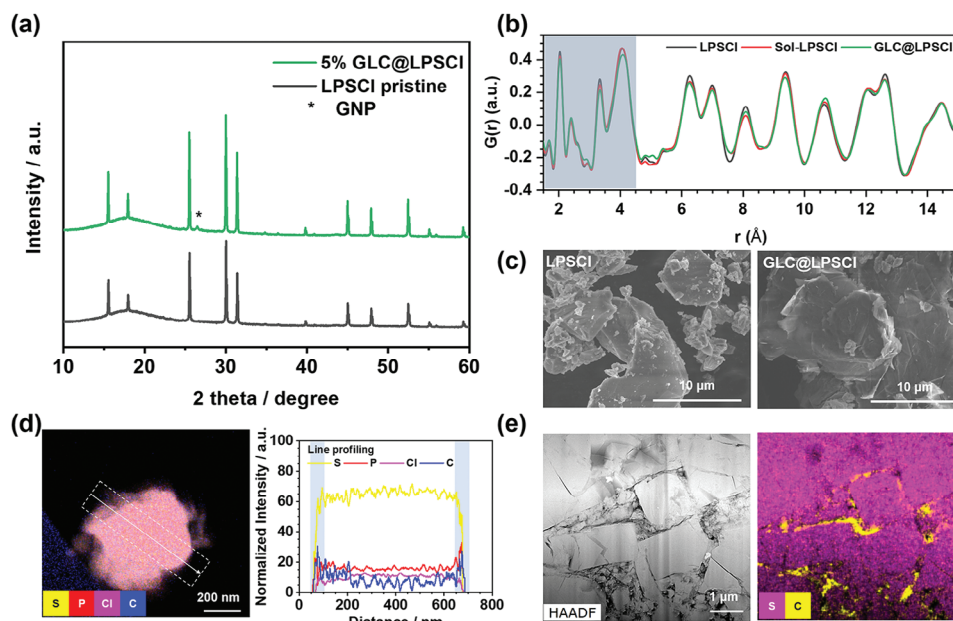
Figure 2. a) XRD results of LPSCl and GLC@LPSCl. b) Reduced PDF, G(r), of LPSCl, solvent-exposed LPSCl (sol-LPSCl), and GLC-coated LPSCl (GLC@LPSCl) in the r ranges of 1.5–15 Å. c) SEM images of the LPSCl electrolyte before and after GLC coating. d) STEM–EDS mapping of the S, P, Cl, and C contents of GLC@LPSCl particle and the corresponding normalized intensity graph along with line profiling. e) HAADF-STEM image and STEM–EDS mapping of the S and C elements in GLC@LPSCl.

in Figure 2b, pristine LPSCl, after solvent exposure (sol-LPSCl), and GLC@LPSCl were each measured, and they exhibited peaks at 2.04, 2.4, 2.62, 3.34, and 4.07 Å, which were attributed to P–S, Li–S/Cl, Li–Li, S–S interchange, and S-S correlation interchange, respectively.[43,44] There was little difference in the peak position, area, and width of LPSCl among the three samples. The results so far have confirmed that no deterioration or structural change from the solvents occurs either on average or locally after coating. This means that there is no chemical side reaction caused by solvent or GNP during the coating process.

Thereafter, SEM analysis was performed to show that the GNP peak detected in XRD was not caused by simple mixing with LPSCl. The SEM image shows that several sheets resembling GNP were attached to the LPSCl surface (Figure 2c). Since the thickness of GNP is random, scanning was performed by lowering the acceleration voltage to 5 kV to mitigate boundary blurring for thin sheet due to volume interaction, and as a result, clear visibility of each sheet boundary was affirmed. In addition, high-angle annular dark field scanning transmission electron microscopy (HAADF-STEM) with energy dispersive X-ray spectroscopy (EDS) was analyzed for a single GLC@LPSCl particle (Figure 2d). In EDS mapping results, the elements corresponding to P, S, and Cl were detected, which means the single particle shown in the HAADF-STEM image is LPSCl. Since C is also detected around LPSCl, it can be considered as GNP coated on LPSCl (Figure S7, Supporting Information). Line profiling was also performed in the direction indicated on the particle as shown in Figure 2d obtaining the normalized relative ratio of each element. Through the increase in the intensity of C at the outermost edge of LPSCl, it was confirmed that LPSCl was wrapped by GNP.

To improve the electronic conductivity in the composite cathode, C must be continuously connected along the SE grain boundary when GLC@LPSCl is introduced into the electrode. To assess this, specimens were prepared by ion milling using a focused ion beam after pelletizing pristine LPSCl and GLC@LPSCl, respectively; subsequently, TEM analysis was performed. The distribution of C in the pellet was visualized using HAADF-STEM and EDS analysis. In the case of pristine LPSCl, naturally, any elements do not exist at the SE interface (or grain boundaries), and in particular, C is barely detected, showing that electron movement hardly occurs between SEs (Figure S8a, Supporting Information). However, in the case of GLC@LPSCl as shown in Figure 2e and Figure S8b (Supporting Information), C was detected at the LPSCl interface (or grain boundaries), confirming the formation of electronic conductivity. Along with detected C in EDS, the inter-planar spacing of that was measured with high resolution (HR) -TEM. The theoretical lattice spacing of Gr is ≈0.34 nm corresponding to d$_{200}$, and since it matches exactly 26.4° with the (002) peak in XRD, the measured inter-planar distance value should be ≈0.34 nm.[45] However, unfortunately, the actual measured value is 0.32–0.36 nm of lattice space, which is due to the difference depending on the number of GLC layers or image drift from the volatilization of SE caused by beam damage.[46]

The ultimate purpose of manufacturing GLC@LPSCl is to improve the electronic conductivity of the SE, thereby addressing the imbalance between electronic and ionic conductivity within the composite cathode. Therefore, as an effect of GNP coating, the resistance and conductivity were measured using the chronoamperometry (CA) method with nonblocking cells to assess whether the electronic conductivity of GLC@LPSCl is improved compared to LPSCl (**Figure 3a**).[47] The current term (I) was averaged for the last 100 points of the measured current value when a constant voltage (V) was applied. The resistance term (R)
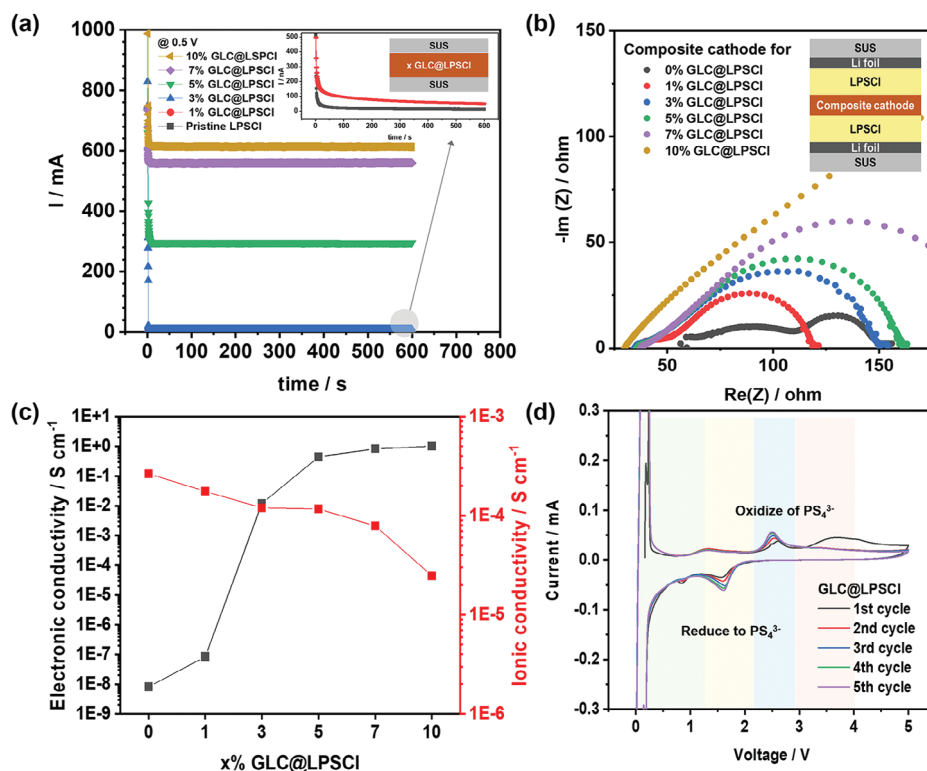
**ADVANCED
SCIENCE NEWS**

www.advancedsciencenews.com

**ADVANCED
ENERGY
MATERIALS**

www.advenergymat.de

Figure 3. a) CA measurement of x% GLC@LPSCl (x = 0, 1, 3, 5, 7, and 10) with a nonblocking cell of [SUS|x% GLC@LPSCl|SUS] configuration at a constant voltage 0.5 V. The inset in this figure shows an enlarged y-axis scale in the range of 0–500 nA to distinguish the pristine LPSCl and 1% GLC@LPSCl. b) Magnified Nyquist plot of the electron-blocking cell of the [Li foil|LPSCl| composite cathode|LPSCl|Li foil] configuration for various composite cathode comprising 70 wt.% of NMC811 and 30 wt.% of x% GLC@LPSCl in a frequency range of 5 MHz–10 mHz. c) Calculated electronic conductivity (black line graph) and relative ionic conductivity (red line graph) of x% GLC@LPSCl from (a) and (b), respectively. d) CV curves of GLC@LPSCl for the first five cycles in a voltage range of 0–5 V (vs Li/Li$^+$) at 0.1 mV s^{-1}; the y-axis range was limited to −0.3 to 0.3 mA.

was calculated using Ohm's law (R = V/I formula), and the conductivity value ($\sigma_{e,x}$) was obtained according to Equation (1) below considering the thickness (l) and area (S) of the pellet.

$$\sigma_{e,x} = \frac{l}{S} \times \frac{1}{R} = \frac{l}{S} \times \frac{I}{V} \tag{1}$$

The electronic conductivity depending on GNP content (x%) was calculated based on the result of applying a voltage of 0.5 V, and the values are summarized in Table S2 (Supporting Information). The electronic conductivity of pristine LPSCl ($\sigma_{e,0}$) was calculated to be 8.14 × 10^{-9} S cm^{-1}, considered as nonconductors, and $\sigma_{e,1}$ also showed very low electronic conductivity increasing by only one order. On the other hand, at GNP content of 3 wt.% or more, it rapidly increased by more than six orders, reaching 1.20 × 10^{-2} and 4.43 × 10^{-1} S cm^{-1} at $\sigma_{e,3}$ and $\sigma_{e,5}$, respectively. Thereafter, as the growth scale had decreased, $\sigma_{e,7}$ and $\sigma_{e,10}$ had very high values of 8.28 × 10^{-1} and 1.01 S cm^{-1}, respectively. The rapid increase in electronic conductivity can be assessed by the presence of an excess of GNPs, and an excess of GNPs can rather hinder ionic conduction. Here, to decide the appropriate ratio of GNP in GLC@LPSCl, we further investigate effective ionic conductivity ($\sigma_{ion,x}$) for composite cathode.

The ion transport resistance of the composite cathode was measured by the electrochemical impedance spectroscopy (EIS)

method using an electron-blocking cell which is composed of [Li foil | LPSCl | composite cathode | LPSCl | Li foil].[46] As shown in Figure 3b, the overall impedance increased depending on increasing GNP contents, and the Nyquist plot for the entire scale is shown in Figure S9a (Supporting Information). Despite being an electron-blocking cell, the impedance could not be measured with GLC@LPSCl alone, so we compared the relative ionic conductivity using a composite cathode which made up 70 wt.% of single crystalline LiNi$_{0.8}$Mn$_{0.1}$Co$_{0.1}$O$_2$ (NMC811) with 30 wt.% of x% GLC@LPSCl. In addition, as a reference cathode, a composite cathode without any conductive materials including GNP was set as 0% GLC@LPSCl. As shown in the electron-blocking cell configuration, Li-ion transport takes place both in the bulk region of the SE layer and in the region within the composite cathode. That is, the overall resistance ($Z_{overall}$) includes the resistance of the SE layer (R_{bulk}) and composite cathode ($Z_{composite}$). If the interfacial resistance can be negligible, the total resistance follows Equation (2).[48,49]

$$Z_{overall} = R_{bulk} + Z_{composite} \tag{2}$$

Additionally, in the case of $Z_{composite}$, the electron and Li ions within the composite cathode showed different movements in $Z_{composite}$ each at high frequency and low frequency. At high frequencies, electrons move in parallel in the opposite direction of

**ADVANCED
SCIENCE NEWS**
www.advancedsciencenews.com

**ADVANCED
ENERGY
MATERIALS**
www.advenergymat.de

Li-ion movement. Particularly, when the electron transport resistance is much smaller than the ion transfer resistance, this $Z_{composite,Hf}$ becomes negligible. In this study, the electronic conductivity of GLC@LPSCl is excellent due to GNP, we ignored the electron transport resistance term. On the other hand, there is only Li-ion movement at low frequency, so Li-ion transport resistance is dominant. In this regard, Equation (2) can be rearranged as the following Equation.

$$Z_{overall,\ Hf} = R_{bulk} \qquad (3)$$

$$Z_{overall,\ Lf} = R_{bulk} + R_{ion} \qquad (4)$$

$$\sigma_{ion,x} = \frac{l}{S} \times \frac{1}{R_{ion}} \qquad (5)$$

To calculate the ionic conductivity within the composite cathode, the value of R_{ion} should be obtained, which can be obtained by subtracting Equation (3) from Equation (4). Therefore, among the measured impedance of x% GLC@LPSCl, the R_{ion} value was obtained by subtracting the high-frequency resistance value ($Z_{overall,Hf}$) from the low-frequency resistance value ($Z_{overall,\ Lf}$), and each ionic conductivity was calculated using Equation (5). The details of the relevant values of $Z_{overall,Hf}$ and $Z_{overall,Lf}$, the Li-ion transport resistances, and calculated effective ionic conductivity are listed in Table S3 (Supporting Information). Interestingly, more than two depressed semicircles were visible in the impedance Nyquist plot of 0% GLC@LPSCl. This is considered to be Li transport resistance resulting from increased surface reaction due to increased interfacial contact between the CAM and SE and includes both the interlayer interface of SE layer–Cathode and the inter-particle interface of CAM–SE.[50] Because it includes non-negligible interfacial resistance, it is not appropriate to use the above Equations (3)–(5) for calculating ionic conductivity. Therefore, the impedance was fitted to an equivalent circuit including all interfaces, and the ionic conductivity was obtained by considering the resistance corresponding to the cathode (Figure S9b, Supporting Information).[51]

The electronic conductivity and ionic conductivity of the GLC@LPSCl according to the GNP content calculated previously are plotted in Figure 3c. As the GNP content increased, electronic conductivity improved, but ionic conductivity decreased, as expected. Because both 3% GLC@LPSCl and 5% GLC@LPSCl have high electronic and ionic conductivities, therefore, they are considered appropriate candidates. Although the ionic conductivity is similar, the electronic conductivity of 5% GLC@LPSCl is slightly higher, hence, it was judged appropriate to conduct the electrochemical evaluation with 5% GLC@LPSCl. Again, all mentioned of GLC@LPSCl from now on refer to 5% GLC@LPSCl.

We confirmed through TEM that GLC@LPSCl was well formed, and as a result, the electronic conductivity was also improved. Furthermore, to investigate whether there is a side reaction occurring during the electrochemical reaction by GNP in intimate contact with LPSCl, a cyclic voltammetry (CV) test was performed using a Li anode as a counter electrode with GLC@LPSCl on the cathode side. As shown in Figure 3d, there was only a reversible reaction of PS_4^{3-} reduction/oxidation ≈1.6 and 2.5 V in addition to the peak of Li insertion/extraction in the GLC matrixes ≈0.1–0.2 V (see arrow in Figure S10a, Supporting Information), whereas no other peak related to the degradation of the SE appeared. So far, there have been some reports that unstable interfaces are formed by side reactions when carbon and sulfide SE composites are operated by CV.[52] When we also evaluated the CV test of 5 wt.% VGCF with 95 wt.% LPSCl in line with C content in GLC@LPSCl, as the cycle progressed, the overcurrent and noise occurred during oxidation (Figure S10b, Supporting Information). Through this, we concluded that there would be little effect on cell performance degradation even with GNP coating on SE.

2.3. Electrochemical Performance of the GLC@LPSCl Composite Cathode

The effectiveness of GLC@LPSCl in improving cell performance compared to ordinary composite cathode was evaluated by using galvanostatic charge–discharge measurement. For the electrochemical cell evaluation, the composite cathode of GLC@LPSCl cell was prepared by mixing 70 wt.% of NMC811 and 30 wt.% of GLC@LPSCl accounting for 1.5 wt.% GNP, a conductive carbon, relative to total mass, while composite cathode of VGCF–LPSCl was composed of 70 wt.% of NMC811, 27 wt.% of LPSCl, and 3 wt.% VGCF, which is intended to consistent with previous research and to show the performance improving apparently. In the cell setup, the cell, along with the composite cathode, used pristine LPSCl—not GLC@LPSCl—as the SE layer and In-Li alloy as the anode, forming a composite cathode/LPSCl/In-Li alloy configuration for electrochemical evaluation. As shown in **Figure 4a**, the initial capacity of GLC@LPSCl and VGCF–LPSCl cell at 0.05 C are similar to 193.43 and 192.02 mAh g^{-1} but Coulombic efficiency (CE) are quite different with 82.7% and 71.8%, respectively. This is because the GLC of GLC@LPSCl prevented direct contact between the NMC active material and LPSCl SE, as well as mitigated electrolyte oxidation. Furthermore, even after GNP coating, the SE surface, which may be exposed during the composite cathode preparation process, may contact the cathode surface and subsequently oxidize the LPSCl. Therefore, LiNbO$_3$ was coated on NMC811 (Nb@NMC811) because it is good at suppressing interfacial side reactions, when Nb@NMC811 is adopted as CAMs, it can deliver more improved initial capacity of 206.09 mAh g^{-1} and CE of 85.3% at 0.05 C.

In addition to the above, we assessed various types of carbon in the same manner with 3 wt.% of carbon content in the composite cathode, and various carbon is depending on dimension (D) including Super P (0D), VGCF (1D), and GNP (2D) (See Figure S11, Supporting Information). The initial CE of the cell without carbon, namely with only NMC811 and LPSCl in a ratio of 70:30 wt.%, had the highest, with 78.4%, following the other research results showing that carbon affects the promotion of side reactions at the CAM–SE interface. Although carbon-free has the highest CE, however, it has a lower specific capacity showing 176.23 mAh g^{-1} than 186.65 mAh g^{-1} with 73.2% for Super P due to lack of electronic conductivity. More interestingly, in the case of cells using GNP simply mixed rather than coated to GLC@LPSCl, the initial CE was as high as carbon-free, but the capacity was much lower than it. Due to the aggregating property of GNPs, it is hard to sufficiently disperse them within a
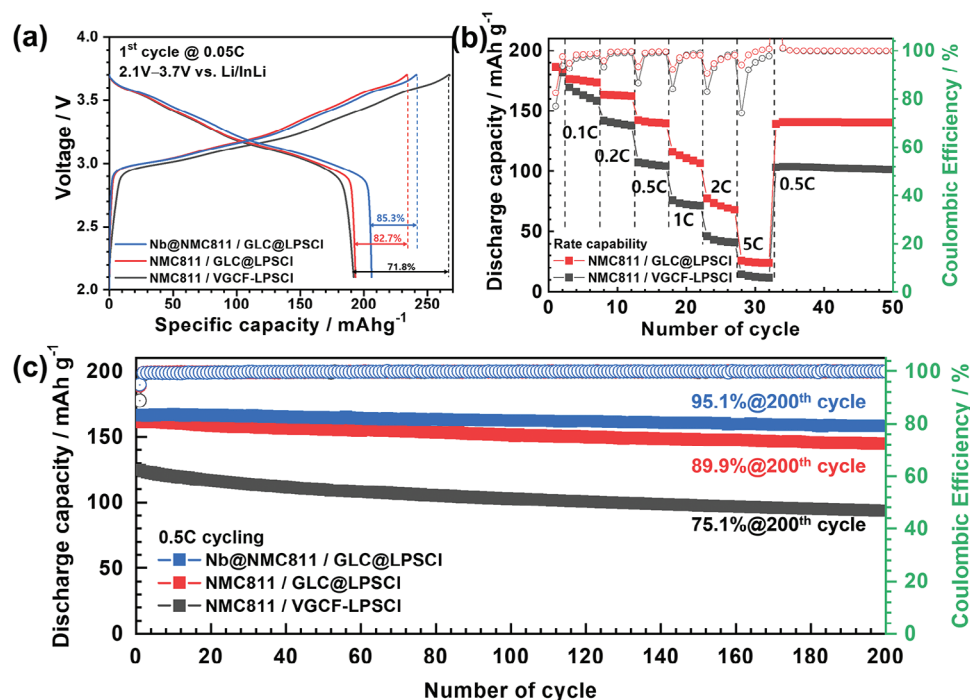
ADVANCED
SCIENCE NEWS
www.advancedsciencenews.com

ADVANCED
ENERGY
MATERIALS
www.advenergymat.de

Figure 4. Galvanostatic charge–discharge test in the range of 2.1–3.7 V (vs InLi/Li$^+$) for the GLC@LPSCl and VGCF–LPSCl composite cathodes. a) First cycle curves with a 0.05 C (9 mA g^{-1}) current density of the NMC811/VGCF–LPSCl, NMC811/GLC@LPSCl, and Nb@NMC811/GLC@LPSCl cells. b) Rate-capability test at several currents, from 0.05 to 5 C, for NMC811/VGCF–LPSCl and NMC811/GLC@LPSCl. c) Comparison of the capacity retentions at a 0.5 C (90 mA g^{-1}) rate up to the 200th cycles of the NMC811/VGCF–LPSCl, NMC811/GLC@LPSCl, and Nb@NMC811/GLC@LPSCl cell.

composite cathode by a simple mixing method. Therefore, GNP not only failed to form a percolating electron pathway but also acted as a bottleneck in the ionic transport pathway resulting in significantly lower specific capacity. From the evaluating initial electrochemical property, among ordinary conductive agents, VGCF showed the most stable performance, so it was used for testing the rate capability and cycling characteristic as VGCF–LPSCl cell compared with GLC@LPSCl cell.

The rate capability was tested for VGCF–LPSCl and GLC@LPSCl. After the formation step with two cycles at 0.05 C, the charge–discharge current density first increased from 0.1 C (18 mA g^{-1}) to 5 C (900 mA g^{-1}) with every five cycles before returning to 0.5 C for additional cycling until the 50th cycle. As shown in Figure 4b, the discharge capacity of GLC@LPSCl was shown to be superior to that of VGCF–LPSCl and there was a little decrease in CE where in the rate changed section. The rate capability is fairly affected by electron transport properties, and the better the electronic conductivity, the lower the charge-transfer resistance. In other words, the excellent rate capability of GLC@LPSCl indicates the formation of percolating network for electron transport in the composite cathode. In addition, thanks to the continuous electron pathway, charge transfer within the electrode becomes smooth, improving utilization of CAM to enhance the capacity even at high current density, making it advantageous for fast charging or high-loading electrode applications.

Figure 4c shows the results of cycling stability for NMC811/VGCF–LPSCl, NMC811/GLC@LPSCl, and Nb@NMC811/GLC@LPSCl cells to 200 cycles at 0.5C cur-

rent density. In the case of VGCF–LPSCl, the capacity retention was 75% after 200 cycles, but GLC@LPSCl showed almost 90% capacity retention after 200 cycles. The corresponding dQ/dV curve with voltage featured the transformation of NMC811 with VGCF–LPSCl or GLC@LPSCl (See Figure S12, Supporting Information). The peak intensity at 0.1C and 0.5C of VGCF–LPSCl was lower than 0.05C even in the 1st cycle. This is considered due to the lack of electronic conductivity in the composite cathode. Furthermore, with an increase in cycle number to 200th cycle at 0.5 C in VGCF–LPSCl, both cathodic and anodic peak intensity decreased continuously, showing poor cyclic reversibility. This is interpreted as being caused by interfacial side reaction,[53] and it is expected that there is also partial acceleration of CAM deterioration resulting from inhomogeneous reactivity. On the other hand, GLC@LPSCl showed that the peak position and intensity overlapped well and the phase transformation was well maintained even as the current density and cycle number increased. In this regard, thanks to further alleviating the interfacial side reaction, 95% capacity retention was achieved in Nb@NMC811/GLC@LPSCl after 200 cycles.

As a result, the GLC@LPSCl cell not only delivers high capacity at high current density, it also improves the cycling characteristics. This is due to a well-developed percolating electron pathway, alleviating inhomogeneous reactivity, and reducing interfacial side reaction between CAMs and SE. The high capacity even at high current density is because inhomogeneous reactivity alleviates by enhancing the balance between ionic and electronic transport besides electronic conductivity improved within the composite cathode through GNP coating. In addition, the
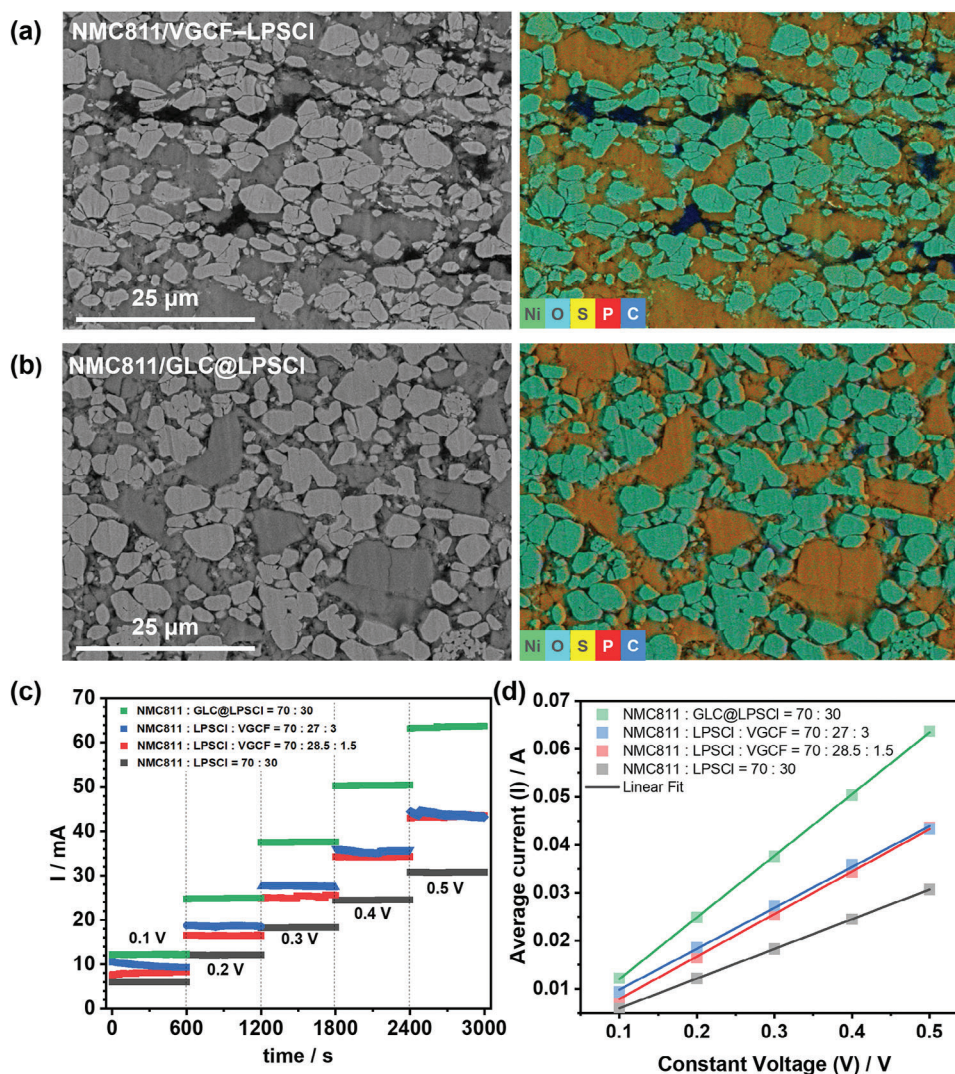
ADVANCED
SCIENCE NEWS

www.advancedsciencenews.com

ADVANCED
ENERGY
MATERIALS

www.advenergymat.de

Figure 5. Cross-sectional SEM images along with the EDS mappings of layered image for the Ni, O, S, P, and C elements of a) NMC811/VGCF–LPSCl and b) NMC811/GLC@LPSCl cells, where the carbon contents were 3.0 and 1.5 wt.%, respectively. c) CA measurement results for each composite cathode composition at 0.1–0.5 V. d) I–V curves with linear fitting for calculating the electronic conductivities of the composite cathode.

inhomogeneous reactivity causes capacity reduction due to the generation of isolated active materials that do not participate in the (de)lithiation reaction.[20,22] By reducing isolated active materials, as much as utilized in electrochemical reactions while minimizing over-charge and -discharge parts, cycling characteristics can also be improved. Another positive effect of GNP coating on SE for improving cycling is due to the reduction of side reactions that can occur at the CAM–SE interface by minimizing direct contact. The reduction of side reactions that can occur at the CAM–SE interface by minimizing direct contact is also the positive effect of GNP coating on improving the cycling characteristic.

2.4. Effects of the Electron-Percolating Pathway on the Cell Performance

From the electrochemical evaluation results, we confirmed that GLC coating makes GLC@LPSCl have high capacity and excel-

lent cycling characteristics. So, we investigated two perspectives on the reasons that could have led to such results, one is for the enhancement of capacity, and the other is for the enhancement of cycling characteristics.

When GLC is well coated on LPSCl, the electron pathway in the composite cathode forms a 3D conductive networking to sufficiently support the movement of fast Li ions, enabling high capacity even at high current density. We conducted cross-sectional milling of the composite cathode for the VGCF–LPSCl cell and GLC@LPSCl cell in a cryogenic environment, confirmed the distribution of carbon, and predicted the flow of electrons accordingly, through SEM-EDS analysis. In general, well-dispersed VGCF in the form of a wire connects separated CAMs from each other to provide electronic conductivity. However, as shown in **Figure** 5a and Figure S13a (Supporting Information), there are many bundled VGCF within the composite cathode, and if insulator SE is located at the end of the carbon, the CAM will not receive electrons anymore, being a blackout region. On the other
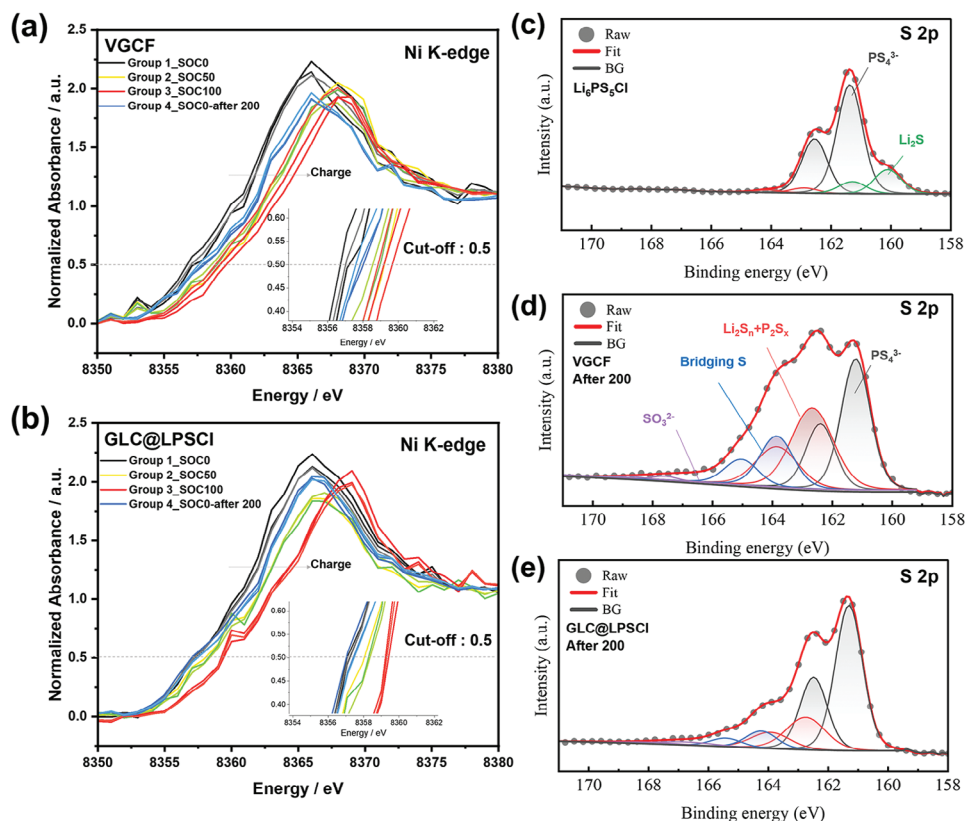
**ADVANCED
SCIENCE NEWS**

www.advancedsciencenews.com

**ADVANCED
ENERGY
MATERIALS**

www.advenergymat.de

Figure 6. XANES spectra of the a) VGCF–LPSCl and b) GLC@LPSCl cells obtained by the TXM–XANES analysis of the Ni K-edge energy change with respect to SOC0, 50, and 100 of the 1st charge and SOC0 after the 200th cycle. XPS results of the S 2p peak for c) LPSCl and after the 200th cycle for the d) VGCF–LPSCl and e) GLC@LPSCl cells.

hand, when GLC@LPSCl is blended with the CAM, GNP playing a role as a conductive pathway is located on the SE surface or between SEs, as shown in Figure 5b, Figures S13b and S14 (Supporting Information). In this way, when carbon is located according to the distribution of the SE, electrons can move continuously through the carbon covering the SE whatever the CAMs are separated from each other. Since no more electron conduction occurs in the electron pathways disconnected area in the VGCF–LPSCl cell, the GLC@LPSCl cell can freely supply electrons to the composite cathode through the continuous electron pathway, therefore it has higher electronic conductivity of the composite cathode than the VGCF–LPSCl cell.

The CA in the same way as in Figure 3a was conducted to confirm the electronic conductivity of the GLC@LPSCl composite cathode. The current value measured for 10 min in 0.1 V increment from 0.1–0.5 V is depicted in Figure 5c, and the average current values of the last 100 points for each voltage are plotted in Figure 5d calculating electronic conductivity through linear fit. For comparison with GLC@LPSCl, VGCF–LPSCl in 1.5 and 3.0 wt.% of VGCF and carbon-free were measured in the same way, respectively. As a result, the composite cathode for carbon-free showed a conductivity of 18.4 mS cm^{-1}, which was higher than the previous study results of 0.3 mS cm^{-1}.[47] The smaller the particle size of the cathode, the better the electronic conductivity.[54] Thanks to the single crystalline morphology cathode with a small particle size of ≈3 μm, it was higher than the literature value

based on 8–10 μm poly NMC with 2 wt.% Super P.[47] VGCF–LPSCl in 1.5 and 3.0 wt.% of VGCF showed similar values of 24.7 and 26.5 mS cm^{-1}, respectively, while GLC@LPSCl showed the highest electronic conductivity of 36.8 mS cm^{-1}, about twice that of carbon-free. When an appropriate amount of carbon is added, the electronic conductivity is improved by about 1.5 to 2 times compared to without carbon, and this demonstrates that the improvement in electronic conductivity effectively acts to increase the initial discharge capacity corresponding with the results shown in Figure 4a and Figure S11 (Supporting Information). In other words, GLC@LPSCl showed high electronic conductivity even with a small amount of carbon through the percolating electron pathway, confirming that electrical conductivity plays an important role in increasing capacity.

The cycling characteristics and its dQ/dV data can help to infer that CAM utilization was improved due to the continuous electron pathway. That means, this can be interpreted that the well-developed percolating electron pathway improves capacity retention by alleviating inhomogeneous reactivity. A local overcharge–discharge area stemming from a heterogeneous reaction results in a decrease in capacity retention as the active material is inactivated. **Figure 6a,b** is the result of TXM–XANES analysis of Ni K-edge energy change concerning the state of charge (SOC) of VGCF–LPSCl and GLC@LPSCl to evaluate the reaction uniformity. Since both VGCF–LPSCl and GLC@LPSCl went through the formation step to make the SOC0 state, there is

a slight difference in energy value in SOC0. When both cells were charged from SOC0 to SOC50, the Ni K-edge energy increased, indicating that Ni was oxidized (Group 2 in the figure). For the VGCF–LPSCl, even though it was charged up to SOC100, the energy value did not increase significantly compared to SOC50, showing no distinct energy gap between group 2 and group 3 (Figure 6a). On the other hand, when GLC@LPSCl was further charged from SOC50 to SOC100, the energy value of each group increased similarly, resulting in a clear difference in groups 2 and 3 (Figure 6b). In other words, the VGCF–LPSCl showed inhomogeneous reactivity even within the 1st cycle, but GLC@LPSCl had a homogeneous reactivity. Therefore, it was confirmed that the formation of a good electron pathway by continuous carbon contact can relieve the inhomogeneous reactivity in the composite cathode. Furthermore, in the discharge state after 200 cycles (see group 4 in the figure), it had a slightly higher energy value than group 1 for VGCF–LPSCl, while the GLC@LPSCl was similar to that of group 1. This highlights that the improvement in cycling characteristics of the GLC@LPSCl is due to the cathode remaining reversibility even after 200 cycles.

In addition to the utilization of CAM, mitigating the interface deterioration, which minimizes the direct contact between the CAM and SE, also improved capacity retention. After the electrochemical test, the cathode surface of VGCF–LPSCl and GLC@LPSCl after 200 cycles were analyzed by XPS to evaluate interfacial side reaction and SE deterioration in the composite cathode. The pristine LPSCl powder had only PS_4^{3-} main peak and the synthetic by-product Li_2S peak as shown in Figure 6c. In the case of VGCF–LPSCl, the main peak of PS_4^{3-} was still clearly visible after 200 cycles, but the peak of polysulfide $Li_2S_n+P_2S_x$ increase significantly with the increase in bridging S (S^0) (Figure 6d). On the other hand, in case of GLC@LPSCl, some $Li_2S_n+P_2S_x$ and S^0 were formed, but the intensity was remarkably lower than that of VGCF–LPSCl (Figure 6e). The XPS analysis result suggests that GLC coating suppressed the formation of by-products from interfacial side reaction. This is because the GLC layer covered on the surface of LPSCl reduces the direct contact area between the CAM and the SE, thereby suppressing side reactions and oxidation of the SE. This is also supported by EIS analysis with cycling as shown in Figure S15 (Supporting Information). For the EIS results in the 1st charge and 200th charge of both cells, the VGCF–LPSCl increases significantly interfacial resistance, especially between CAM–SE after 200 cycles, while GLC@LPSCl showed a slight increase in resistance even after 200 cycles. In other words, the XPS and EIS results led to the same conclusion, thanks to the GLC coating, the chance of SE decomposition on the CAM surface is reduced, thereby suppressing an increase in interfacial resistance.

As mentioned above, the ultimate goal of GLC coating on the SE for the formation of a percolating electron pathway is to fabricate high-performance ASSBs even through thick and high-loading-level electrodes. When the loading amount was simply increased to enhance the cell capacity (not just for specific capacity) in the VGCF–LPSCl composite cathode, the inhomogeneous reactivity became more severe owing to the increased current density, and the capacity decreased rapidly.[26,27]

To confirm that the improvement in electronic conductivity through the formation of the percolating electron pathway is effective for obtaining capacity even in high-loading thick electrodes, the cell test was performed after increasing the loading amount of the composite cathode four times from 10.5 mg (7.92 mg cm^{-2}) to 42 mg (31.65 mg cm^{-2}) as shown in **Figure 7**. As a result, at a relatively low current density of 0.285 mA cm^{-2} (0.05 C), both the VGCF–LPSCl cell and the GLC@LPSCl cell showed similar initial discharge capacities of 184 mAh g^{-1} (7.7 mAh), but in case of at a high current density of 2.85 mA cm^{-2} (0.5 C), the capacity of GLC@LPSCl cell had 5.34 mAh maintaining 69.1% compared with 0.05 C (0.5/0.05 C), which was ≈1.37 times higher than that of the VGCF–LPSCl cell (50.3%) (Figure 7a). The thicknesses of the VGCF-LPSCl/HL and GLC@LPSCl/HL composite cathodes are 208 and 195 μm, respectively (See Figure S16, Supporting Information). Based on these values, the volumetric energy density of the composite cathodes is calculated to be 1034 and 1102 Wh L^{-1}, respectively. Additionally, even after 100 cycles, GLC@LPSCl showed a capacity retention of 75.1% and showed better cell performance than VGCF–LPSCl (48.5%) (Figure 7b). Consistent with the results so far, this result indicates that the rapidly decrease cell performance at high current densities of the VGCF–LPSCl cell is due to the low electronic conductivity of the composite cathode, which disturbs the smooth movement of electrons and thus cannot manage with the increasing current density. Therefore, to manufacture a high-energy-density ASSB through thick and high-loading electrodes, it is important to improve ionic conductivity, but it is more important to balance ionic–electronic conductivity by providing a percolating electron-conductive pathway.

3. Conclusion

High-performance electric vehicles require the development of high-energy-density ASSBs. However, the conventional composite cathode configuration in sulfide-based ASSBs exhibits disadvantages, such as limited capacity and inadequate cycling characteristics. Additionally, the degradation of the cell performance becomes more severe when a thick electrode is required to increase a real cell capacity at high current density. We assumed this issue was mainly caused by the imbalance between the electronic and ionic conductivities of the battery, which resulted in inhomogeneous reactions within the composite cathode. Thus, we introduced a method comprising GLC coating on the SE rather than CAM to generate a continuous electron-conductive pathway. Thus, GLC@LPSCl was obtained by a simple solvent-based process to avoid heat-induced aggregation, and no additives other than GLC and LPSCl were used. Owing to the coating effect, the GLC@LPSCl cells exhibited higher capacity at 0.5 C than VGCF–LPSCl, and the cycling characteristics improved from 75% to 90% after 200 cycles. The capacity was enhanced by improving the electronic conductivity of the composite cathode by forming an electron-percolating pathway, as well as eliminating the carbon agglomeration and minimizing the electrical disconnection between CAMs. Furthermore, the well-developed electron pathway enhanced the cycling characteristics by inhibiting the inhomogeneous reactions in the cell. Further, it suppressed cathode degradation by eliminating the inactivated cathode material as well as the local overcharge. Moreover, the GLC layer prevents direct CAM–SE interface contact and reduces the interfacial side reactions, contributing to enhanced cycling performance. Finally, we confirmed that the well-developed electron pathway was key to
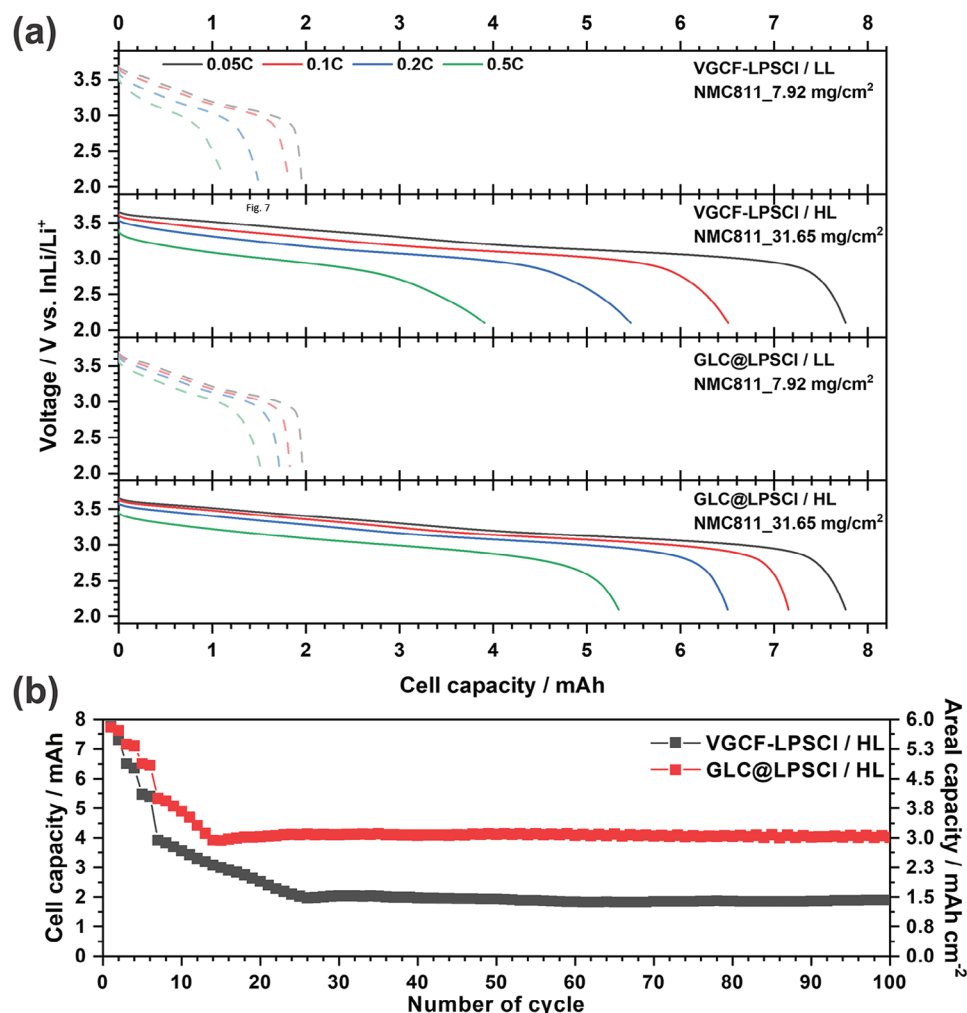
**ADVANCED
SCIENCE NEWS**

www.advancedsciencenews.com

**ADVANCED
ENERGY
MATERIALS**

www.advenergymat.de

Figure 7. a) Comparison of the 1st discharge curve at 0.05, 0.1, 0.2, and 0.5 C of low- and high-loading (LL and HL) amounts of the VGCF–LPSCl and GLC@LPSCl cells. b) Cycling characteristics of the high-loading VGCF–LPSCl and GLC@LPSCl cells evaluated at 0.5 C.

cell performance, especially in thick electrodes. At a high loading, the GLC@LPSCl cell exhibited a capacity retention rate of 75% after 100 cycles and a cell capacity that was two times higher than that of the VGCF–LPSCl cell. This study revealed the criticality of a well-connected 3D electronic network to the development of high-energy-density ASSBs. Simultaneously, to ensure homogeneous reactivity in the cell, the electronic and ionic conductivities of the composite cathode must be balanced, aiming to improve the capacity and cycling characteristics of the battery.

Supporting Information

Supporting Information is available from the Wiley Online Library or from the author.

Acknowledgements

Conflict of Interest

The authors declare no conflict of interest.

Author Contributions

H.-J.S. conceptualized the idea for the study; designed the methodology; performed investigation; and wrote the original draft. J.-T.K. and D.H. performed validation and formal analysis. H.-S.K., J.M., J.K., and K.-W.N. performed supervision and acquired resources. K.Y.C. and H.-G.J. performed funding acquisition and project administration. H.-G.J. wrote, reviewed, and edited the final manuscript

[1] B. Scrosati, *Electrochim. Acta* **2000**, *45*, 2461.
[2] N. Kittner, F. Lill, D. M. Kammen, *Nat. Energy* **2017**, *2*, 17125.
[3] J. Janek, W. G. Zeier, *Nat. Energy* **2016**, *1*, 16141.
[4] C. Wang, J. Liang, Y. Zhao, M. Zheng, X. Li, X. Sun, *Energy Environ. Sci.* **2021**, *14*, 2577.
[5] A. Manthiram, X. Yu, S. Wang, *Nat. Rev. Mater.* **2017**, *2*, 16103.
[6] Y.-G. Lee, S. Fujiki, C. Jung, N. Suzuki, N. Yashiro, R. Omoda, D.-S. Ko, T. Shiratsuchi, T. Sugimoto, S. Ryu, J. H. Ku, T. Watanabe, Y. Park, Y. Aihara, D. Im, I. T. Han, *Nat. Energy* **2020**, *5*, 299.
[7] D. H. S. Tan, Y.-T. Chen, H. Yang, W. Bao, B. Sreenarayanan, J.-M. Doux, W. Li, B. Liu, S.-Y. Ham, B. Sayahpour, J. Scharf, E. A. Wu, G. Deysher, H. E. Han, H. J. Hah, H. Jeong, J. B. Lee, Z. Chen, Y. S. Meng, *Science* **2021**, *373*, 1494.
[8] A. L. Mong, Y. Ahn, R. Puttaswamy, D. Kim, *Energy Mater.* **2023**, *3*, 300035.
[9] B. Phng, Z. Liu, Q. Zhou, S. Xiong, S. Xia, X. Yuan, F. Wang, K. I. Ozoemena, L. Liu, L. Fu, Y. Wu, *Adv. Mater.* **2024**, *36*, 2307142.
[10] Q. Zhou, X. Yang, X. Xiong, Q. Zhang, B. Peng, Y. Chen, Z. Wang, L. Fu, Y. Wu, *Adv. Energy Mater.* **2022**, *12*, 2201991.
[11] A. Banerjee, X. Wang, C. Fang, E. A. Wu, Y. S. Meng, *Chem. Rev.* **2020**, *120*, 6878.
[12] A. Sakuda, A. Hayashi, T. Ohtomo, S. Hama, M. Tatsumisago, *J. Power Sources* **2011**, *196*, 6735.
[13] J. T. Kim, H.-J. Shin, A.-Y. Kim, H. Oh, H. Kim, S. Yu, H. Kim, K. Y. Chung, J. Kim, Y.-K. Sun, H.-G. Jung, *J. Mater. Chem. A* **2023**, *11*, 20549.
[14] J. Haruyama, K. Sodeyama, L. Han, K. Takada, Y. Tateyama, *Chem. Mater.* **2014**, *26*, 4248.
[15] Y. Xiao, L. J. Miara, Y. Wang, G. Ceder, *Joule* **2019**, *3*, 1252.
[16] Y. Lee, J. Jeong, H. J. Lee, M. Kim, D. Han, H. Kim, J. M. Yuk, K.-W. Nam, K. Y. Chung, H.-G. Jung, S. Yu, *ACS Energy Lett.* **2022**, *7*, 171.
[17] Y. Kato, S. Hori, T. Saito, K. Suzuki, M. Hirayama, A. Mitsui, M. Yonemura, H. Iba, R. Kanno, *Nat. Energy* **2016**, *1*, 16030.
[18] S. P. Ong, Y. Mo, W. D. Richards, L. Miara, H. S. Lee, G. Ceder, *Energy Environ. Sci.* **2013**, *6*, 148.
[19] S. Teragawa, K. Aso, K. Tadanaga, A. Hayashi, M. Tatsumisago, *J. Power Sources* **2014**, *248*, 939.
[20] J. Kim, W. Lee, J. Seok, E. Lee, W. Choi, H. Park, S. Yun, M. Kim, J. Lim, W.-S. Yoon, *J. Energy Chem.* **2022**, *66*, 226.
[21] Y. Kimura, A. Tomura, M. Fakkao, T. Nakamura, N. Ishiguro, O. Sekizawa, K. Nitta, T. Uruga, T. Okumura, M. Tada, Y. Uchimoto, K. Amezawa, *J. Phys. Chem. Lett.* **2020**, *11*, 3629.
[22] Y. Nomura, K. Yamamoto, T. Hirayama, E. Igaki, K. Saitoh, *ACS Energy Lett.* **2020**, *5*, 2098.
[23] H.-J. Shin, J. T. Kim, A.-Y. Kim, N. Noh, J. Park, C. R. Park, S. Yu, H. Kim, K. Y. Chung, J. M. Yuk, S.-T. Myung, H.-G. Jung, *Adv. Energy Mater.* **2023**, *13*, 2301220.
[24] M. Otoyama, Y. Ito, A. Hayashi, M. Tatsumisago, *J. Power Sources* **2016**, *302*, 419.
[25] X. Yang, K. D. Davis, X. Gao, X. Sun, *eTransportation* **2022**, *11*, 100152.
[26] M. Singh, J. Kaiser, H. Hahn, *J. Electrochem. Soc.* **2015**, *162*, A1196.
[27] K.-Y. Park, J.-W. Park, W. M. Seong, K. Yoon, T.-H. Hwang, K.-H. Ko, J.-H. Han, Y. Jaedong, K. Kang, *J. Power Sources* **2020**, *468*, 228369.
[28] R. Xu, Y. Yang, F. Yin, P. Liu, P. Cloetens, Y. Liu, F. Lin, K. Zhao, *J. Mech. Phys. Solids* **2019**, *129*, 160.
[29] X. Chen, W. Lu, C. Chen, M. Xue, *Int. J. Electrochem. Sci.* **2018**, *13*, 296.
[30] K.-C. Jiang, S. Xin, J.-S. Lee, J. Kim, X.-L. Xiao, Y.-G. Guo, *Phys. Chem. Chem. Phys.* **2012**, *14*, 2934.
[31] K.-Y. Park, J.-M. Lim, N. S. Luu, J. R. Downing, S. G. Wallace, L. E. Chaney, H. Yoo, W. J. Hyun, H.-U. Kim, M. C. Hersam, *Adv. Energy Mater.* **2020**, *10*, 2001216.
[32] Y. Han, S. H. Jung, H. Kwak, S. Jun, H. H. Kwak, J. H. Lee, S.-T. Hong, Y. S. Jung, *Adv. Energy Mater.* **2021**, *11*, 2100126.
[33] S. W. Park, G. Oh, J.-W. Park, Y.-C. Ha, S.-M. Lee, S. Y. Yoon, B. G. Kim, *Small* **2019**, *15*, 1900235.
[34] F. Walther, S. Randau, Y. Schneider, J. Sann, M. Rohnke, F. H. Richter, W. G. Zeier, J. Janek, *Chem. Mater.* **2020**, *32*, 6123.
[35] J. H. Choi, S. Choi, T. J. Embleton, K. Ko, K. S. Saqib, M. Jo, J. Hwang, S. Park, Y. Son, P. Oh, *Batteries* **2023**, *9*, 590.
[36] W. Zhang, T. Leichtweiß, S. P. Culver, R. Koerver, D. Das, D. A. Weber, W. G. Zeier, J. Janek, *ACS Appl. Mater. Interfaces* **2017**, *9*, 35888.
[37] R. Raccichini, A. Varzi, S. Passerini, B. Scrosati, *Nat. Mater.* **2015**, *14*, 271.
[38] W. Li, D. Li, Q. Fu, C. Pan, *RSC Adv.* **2015**, *5*, 80428.
[39] R. Xu, Z. Wu, S. Zhang, X. Wang, Y. Xia, X. Xia, X. Huang, J. Tu, *Chem. Eur. J.* **2017**, *23*, 1.
[40] Z. Liu, H. Gao, S. Wen, H. Lin, X. Chen, G. Chen, *Appl. Sur. Sci.* **2021**, *567*, 150718.
[41] U. Khan, H. Porwal, A. O'Neill, K. Nawaz, P. May, J. N. Coleman, *Langmuir* **2011**, *27*, 9077.
[42] X. Wang, L. Ye, C.-W. Nan, X. Li, *ACS Appl. Mater. Interfaces* **2022**, *14*, 46627.
[43] S. Shiotani, K. Ohara, H. Tsukasaki, S. Mori, R. Kanno, *Sci. Rep.* **2017**, *7*, 6972.
[44] J. G. Smith, D. J. Siegel, *Nat. Commun.* **2020**, *11*, 1483.
[45] H.-H. Huang, K. K. H. D. Silva, G. R. A. Kumara, M. Yoshimura, *Sci. Rep.* **2018**, *8*, 6849.
[46] M. Nakamura, T. Kawai, M. Irie, R. Yuge, S. Iijima, S. Bandow, M. Yudasaka, *Carbon* **2013**, *61*, 644.
[47] R. Rajagopal, Y. Subramanian, K.-S. Ryu, *RSC Adv.* **2021**, *11*, 32981.
[48] N. Kaiser, S. Spannenberger, M. Schmitt, M. Cronau, Y. kato, B. Roling, *J. Power Sources* **2018**, *396*, 175.
[49] S. H. Kang, J. Y. Kim, D. O. Shin, M. J. Lee, Y.-G. Lee, *Mater. Today Energy* **2022**, *23*, 100913.
[50] D. Shin, J. S. Nam, H. T. L. Nguyen, Y. Jo, K. Lee, S. M. Hwang, Y.-J. Kim, *J. Mater. Chem. A* **2022**, *10*, 23222.
[51] B. Emley, C. Wu, L. Zhao, Q. Ai, Y. Liang, Z. Chen, L. Guo, T. Terlier, J. Lou, Z. Fan, Y. Yao, *Mater. Futures* **2023**, *2*, 045102.
[52] C. Wang, J. Liang, J. Luo, J. Liu, X. Li, F. Zhao, R. Li, H. Huang, S. Zhao, L. Zhang, J. Wang, X. Sun, *Sci. Adv.* **2021**, *7*, 1896.
[53] J. Shi, P. Li, K. Han, D. Sun, W. Zhao, Z. Liu, G. Liang, K. Davey, Z. Guo, X. Qu, *Energy Storage Mater.* **2022**, *51*, 306.
[54] F. Strauss, T. Bartsch, L. D. Biasi, A.-Y. Kim, J. Janek, P. Hartmann, T. Brezesinski, *ACS Energy Lett.* **2018**, *3*, 992.